ACS Catalysis

Research Article

pubs.acs.org/acscatalysis

Design, Synthesis, and Binding Affinity Evaluation of Hoechst 33258 Derivatives for the Development of Sequence-Specific DNA-Based Asymmetric Catalysts

Karen Amirbekyan,[†,‡] Nicolas Duchemin,[§] Erica Benedetti,[§] Rinah Joseph,[§] Aude Colon,[§] Shiraz A. Markarian,[‡] Lucas Bethge,[#] Stephan Vonhoff,[#] Sven Klussmann,[#] Janine Cossy,[§] Jean-Jacques Vasseur,[†] Stellios Arseniyadis,*[,§,¶] and Michael Smietana*[,†]

[†]Institut des Biomolécules Max Mousseron, UMR 5247 CNRS, Université de Montpellier, ENSCM Place Eugène Bataillon, 34095 Montpellier, France

[‡]Department of Physical Chemistry, Yerevan State University, 1 Alex Manoogian, Yerevan 0025, Armenia

[§]Laboratoire de Chimie Organique, Institute of Chemistry, Biology and Innovation (CBI) - ESPCI ParisTech/CNRS (UMR8231)/PSL* Research University, 10 rue Vauquelin, 75231 CEDEX 05 Paris, France

[#]NOXXON Pharma AG, Max-Dohrn-Strasse 8-10, 10589 Berlin, Germany

[¶]School of Biological and Chemical Sciences, Queen Mary University of London, Joseph Priestley Building, Mile End Road, London E1 4NS, United Kingdom

Supporting Information

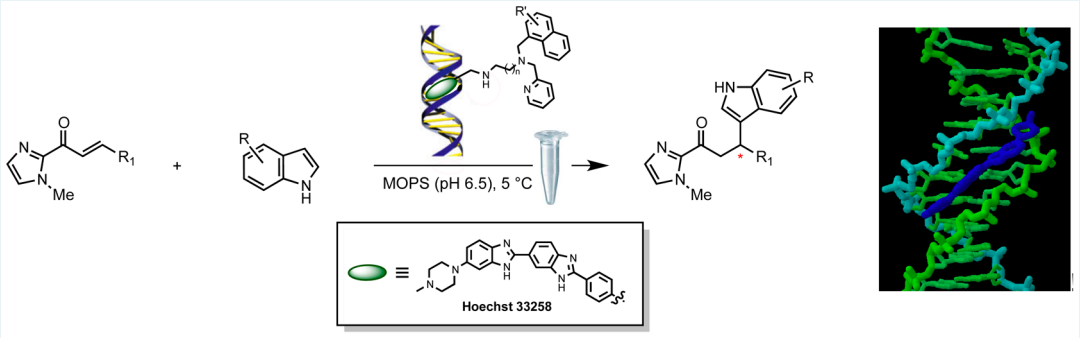

ABSTRACT: To date, the concept of DNA-based asymmetric catalysis has been successfully applied to various synthetic transformations by way of hybrid catalysts involving either an intercalator or an integrated ligand anchored through supramolecular interactions. We report here a new anchoring strategy based on the well-known groove-binder Hoechst 33258. The interaction between calf thymus DNA (ct-DNA) and poly[d(A-T)$_2$] with a series of Hoechst 33258-derived ligands was studied by UV−vis absorption spectroscopy, thermal melting analysis, fluorescence emission, CD spectroscopy, mass spectrometry, and molecular docking. The results clearly show that a groove-binding anchoring strategy can be envisioned for DNA-based asymmetric catalysis, offering additional mechanistic insight on how the intrinsic chirality of DNA can be transferred to a reaction product. Most importantly, this new anchoring strategy offers interesting compartmentalization possibilities and provides a new way to reverse the enantioselectivity outcome of a given reaction.

KEYWORDS: *DNA-based asymmetric catalysis, minor groove binder, Hoechst 33258, Friedel−Crafts, biohybrid catalysis*

INTRODUCTION

The use of artificial metalloenzymes, which combine transition-metal catalysis and biocatalysis, has recently emerged as a promising concept to evolve biomolecular scaffolds into performing new catalytic reactions and/or new functions.[1] While early studies were devoted to the development of artificial metalloproteins and peptides, DNA-based artificial metalloenzymes have recently drawn considerable interest because of their unique features that comprise a chemically stable chiral double helix associated with many programmable secondary structures.[2] The first example of a direct transfer of chirality from natural DNA to a Cu(II) complex all the way to a Diels−Alder reaction product was reported in 2005 by Roelfes and Feringa.[3] Since then, the concept has been extended to many carbon−carbon, carbon−heteroatom, and carbon−halogen bond-forming reactions.[2,4] Motivated by the potential significance of DNA in asymmetric catalysis, our group demonstrated the decisive role of the nature of the helix on

Received: February 18, 2016
Revised: March 29, 2016

DOI: 10.1021/acscatal.6b00495
ACS Catal. 2016, 6, 3096−3105

the enantioselectivity outcome by studying the influence of L- and D-DNA interacting with a Cu(II) bipyridine complex in Friedel–Crafts alkylations and Michael addition reactions.[5] More recently, we even extended the concept of DNA-based asymmetric catalysis to continuous-flow applications by developing a fully recyclable trivial-to-use cellulose-supported DNA-based catalyst.[6] Despite these efforts, the implementation of DNA-based artificial metalloenzymes toward concurrent cascade reactions requires a precise and programmable anchoring of the transition metal into the biomolecular scaffold. Interestingly, all the anchoring strategies reported so far involve either intercalation of the coordination complexes into natural double-strand DNA (ds DNA),[7] second coordination sphere interactions,[8] or covalent attachment of the ligand directly onto the DNA.[9] While the latter allows for precise positioning of the metal complex, it requires the synthesis of modified nucleotides or nucleotide analogues and their incorporation into synthetic oligonucleotides, which hampers any attempt of compartmentalization.

Sequence specific targeting of ds-DNA is a well-known strategy to control the regulation of gene expression,[10] site-directed mutagenesis,[11] and gene repair.[12] In particular, the DNA minor groove is the center of action of a large number of drugs such as the antiviral agents netropsin and distamycin, the anti-*Pneumocystis carinii* drug, pentamidine, and DNA stain Hoechst 33258 (H33258). These molecules interact in AT-rich regions of B form duplex DNA,[13] where they can block the transcription[14] or the action of DNA topoisomerases.[15] Studies by X-ray crystallography and NMR analysis carried out with oligonucleotides of various sequences revealed that four consecutive AT-base pairs are required for H33258 to bind the minor groove of dsDNA.[16] Quantitative DNase I foot printing studies actually showed that AATT represents the strongest affinity binding site for H33258,[17] while biophysical studies performed on poly[d(A-T)$_2$], poly[d(A)·d(T)] and poly[d(G-C)$_2$] revealed the existence of multiple binding modes between the drug and synthetic DNAs.[13b]

Given the high affinity of Hoechst 33258 toward DNA, we became interested in designing structural modifications of H33258 that would confer interesting asymmetric induction capabilities in conjunction with high sequence specificity. Hence, by taking advantage of the free phenolic group of the molecule, we planned to synthesize new bifunctional DNA ligands bearing both a minor groove-binding moiety and a chelating site able to coordinate to a transition metal; both linked to either a rigid or a flexible spacer (Figure 1). Two classes of bifunctional substrates bearing either a benzylic or a propargylic amine were thus devised, synthesized, and eventually evaluated for their catalytic activity. Several techniques including UV–vis absorption spectroscopy, thermal melting analysis, fluorescence emission, CD spectroscopy, mass spectrometry, and molecular docking were employed to monitor their prospective interaction with ct-DNA and poly[d(A-T)$_2$] and various DNA hairpins. Most importantly, we wished to address three key questions: (i) How much binding affinity can be attained? (ii) Will the modifications sustain the AT sequence-selectivity? (iii) What is the correlation between DNA affinity and enantioselectivity outcome? We report here the results of our endeavor.

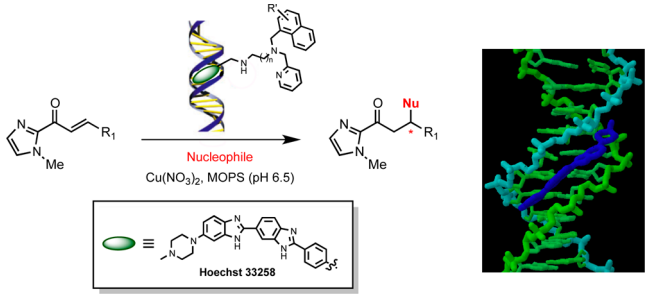

Figure 1. Sequence-specific catalysts for DNA-based asymmetric catalysis.

RESULTS AND DISCUSSION

The first series of bifunctional ligands we wished to prepare contained a minor groove-binding moiety bound to a metal-chelating agent through a flexible benzylamine-type linkage. To access these types of compounds, we therefore needed to introduce an aldehyde moiety to the Hoechst 33258 scaffold (Scheme 1). This was achieved by first converting the phenol

Scheme 1. Synthesis of New Hoechst 33258-Derived Ligands and Representative Structures

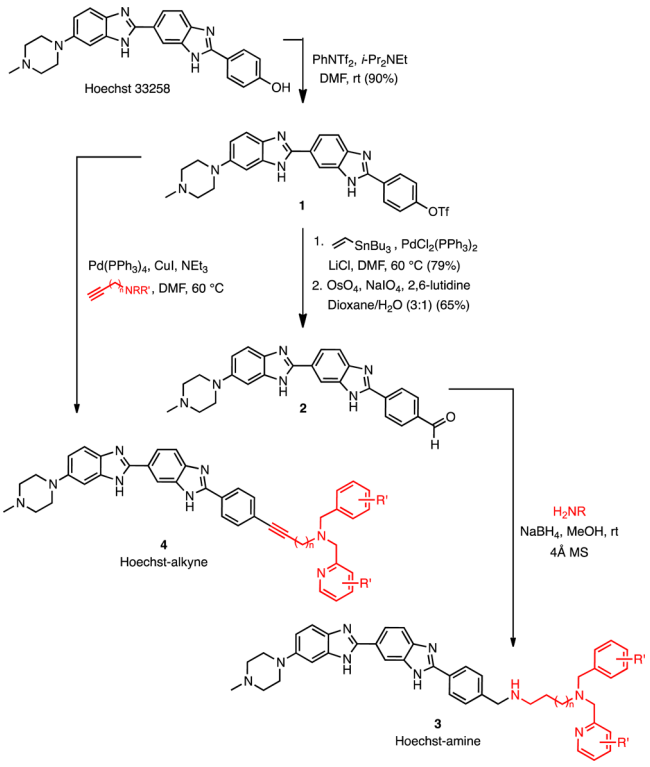

to the corresponding trifluoromethansulfonate by subjecting Hoechst 33258 to *N*-phenyl-bis(trifluoromethane)sulfonimide and diisopropylethylamine. The resulting triflate derivative **1** was then engaged in a Stille coupling with tributyl(vinyl)tin in the presence of LiCl and a catalytic amount of Pd(PPh$_3$)$_2$Cl$_2$ in order to introduce a vinyl moiety, which was subsequently cleaved using osmium tetroxide, NaIO$_4$ and 2,6-lutidine to afford the desired Hoechst-aldehyde precursor **2**. The synthesis of the amine partner began by first monoprotecting commercially available ethylene diamine or 1,3-diaminopropane as the corresponding mono *tert*-butyl carbamates **5a** and **5b** (Scheme 2). These latter compounds were then subjected to a reductive amination with 2-pyridinecarboxalde-

DOI: 10.1021/acscatal.6b00495
ACS Catal. 2016, 6, 3096–3105

Scheme 2. Synthesis of Diamines Bearing a Pendant Pyridine Ring

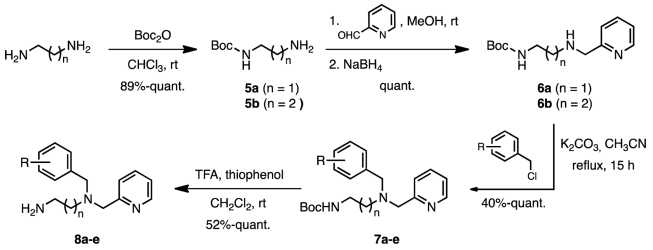

Scheme 3. Synthesis of Propargylamines Bearing a Pendant Pyridine Ring

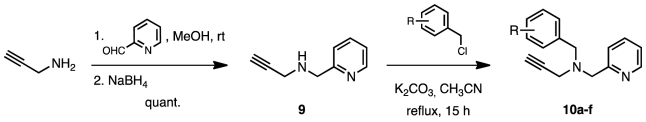

hyde to afford the secondary amines **6a** and **6b** in quantitative yield. Finally, a nucleophilic substitution with the appropriate benzyl chloride followed by the deprotection of the primary amine afforded the desired amines **8a−e** in moderate to excellent yields ranging from 52% to quantitative. With the two coupling partners in hand, the last step of the synthesis involved a reductive amination between aldehyde **2** and the corresponding amines. This was achieved under standard conditions, affording the desired bifunctional Hoechst 33258-derived amine-type ligands **3a−e** in only five steps (longest linear sequence) and yields ranging from 43% to 66% (Figure 2).

In an alternative design, the DNA-binding moiety was linked to the metal-binding domain through a more rigid alkyne type spacer. In this case, the synthesis involved a Sonogashira coupling between Hoechst triflate **1** and several diversely substituted propargyl amines **10a−f**. The latter were obtained following the reaction sequence reported in Scheme 3. Hence, starting from commercially available propargyl amine, a reductive amination with 2-pyridine carboxyaldehyde followed by a nucleophilic substitution with the appropriate benzyl chloride derivative readily afforded the desired propargylic amines, which were finally engaged in the key Sonogashira coupling to afford the desired "Hoechst-alkyne" type bifunctional ligands **4a−f** in good to excellent yields ranging from 61% to 89% (Figure 2).

The affinity of these newly synthesized Hoechst derivatives with DNA was then investigated using various techniques including UV−vis absorption spectroscopy, thermal melting fluorescence, CD spectroscopy, mass spectrometry (see Supporting Information), and molecular docking studies. The results show a strong influence of the type of linkage involved between the Hoechst residue and the metal-binding domain.

UV−vis Absorption Studies. With the objective to study the interaction between our bifunctional ligands and DNA and to assess how the structural modifications influenced the DNA binding affinity, we performed a series of UV−vis absorption studies and compared the results with the ones obtained with Hoechst 33258 (see Supporting Information). The association constant (expressed in molar base pairs) of Hoechst 33258 with ct-DNA and poly[d(A-T)$_2$] are in good agreement with the literature data.[13b] The absorption spectra of the Hoechst derivatives were recorded in the presence of an increasing concentration of ct-DNA, thus providing characteristic dose-dependent curves convenient to describe their interaction (Table 1). The first obvious result obtained from these titrations is that in the 300−420 nm region, the Hoechst-amines exhibit stronger hypochromism (up to 65%) and red shifts than their alkyne analogues.

This was particularly marked for compound **3a**, which induced an extensive broadening in the 310−425 nm region as well as a significant red-shift (916 cm^{-1}) (Figure 3A). Interestingly, this red shift (341−352 nm) was larger than

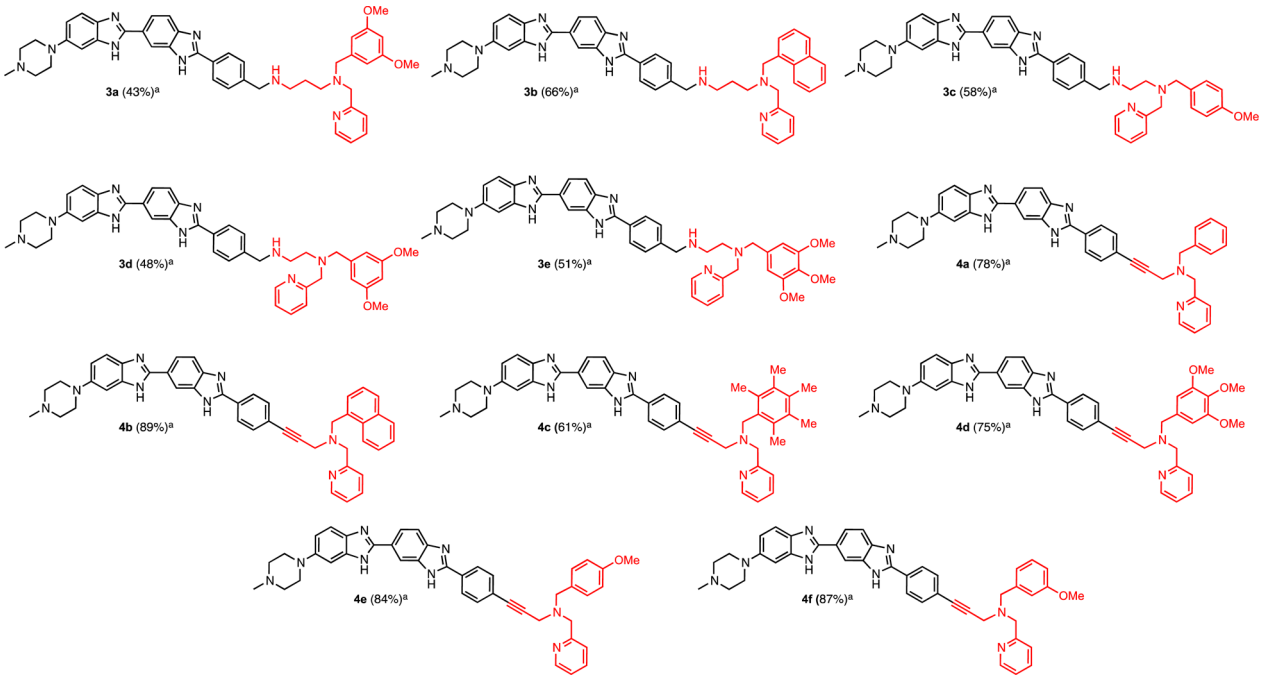

Figure 2. Library of Hoechst 33258-derived ligands. [a]Yields correspond to the final coupling step.

DOI: 10.1021/acscatal.6b00495
ACS Catal. 2016, 6, 3096−3105

Table 1. Spectroscopic Data and Association Constants Obtained for the Probe/ct-DNA Mixtures Studies from UV−vis Titration (Cacodylate Buffer, pH 7.4, 25 °C)

compound	λ_{max} free (nm)	λ_{max} bound (nm)	ΔE (cm^{-1})	% hypochromism(wavelength, nm)	ε_{free} ($M^{-1}cm^{-1}$) at λ_{max} free	ε_{bound} ($M^{-1}cm^{-1}$) at λ_{max} bound	$K_a/10^6$, M^{-1}
3a	341	352	916	65 (341)	25500	8920	3.24 (±0.3)
3a[a]	345	357	974	41 (345)	22300	13160	2.85 (±0.3)
3b	344	352	661	62 (344)	24500	9310	2.40 (±0.2)
3b[a]	347	356	728	38 (347)	21100	13080	1.90 (±0.2)
3c	340	349	758	45 (340)	19500	10730	1.00 (±0.1)
3d	338	346	684	55 (338)	21250	9560	1.20 (±0.1)
3e	343	348	419	60 (343)	25000	10000	1.60 (±0.1)
4a	355	358	236	8 (355)	28750	26450	0.15 (±0.02)
4b	352	358	476	17 (352)	25750	21370	0.75 (±0.1)
4b[a]	354	361	548	12 (354)	23400	20590	0.68 (±0.1)
4c	350	354	323	14 (350)	22450	19310	0.65 (±0.05)
4d	355	360	391	12 (355)	18500	16280	0.54 (±0.03)
4e	347	354	570	10 (347)	22570	20540	0.35 (±0.03)
4f	349	357	640	9(349)	20600	18950	0.28 (±0.01)

[a]Data corresponding to binding with ct-DNA in the presence of one equivalent of Cu^{2+}.

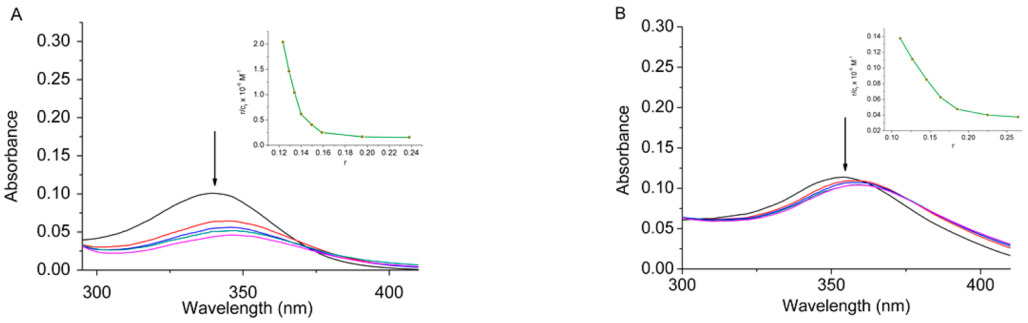

Figure 3. UV−vis absorption spectra of compound **3a** (A) and **4a** (B) in the absence (black) and in the presence of increasing concentration of ct-DNA. The arrows show the decrease in absorbance at 341 and 355 nm (for **3a** and **4a**, respectively). Experimental conditions: 4 μM initial concentration of ligands, [ct-DNA] = 0−32 μM, 100 mM NaCl, 10 mM sodium cacodylate, pH 7.4, 25 °C. Insets: Scatchard plots for the binding of compounds **3a** and **4a** with ct DNA obtained from UV−vis titration data.

the one observed with Hoechst 33258 under otherwise identical conditions (340−345 nm, see Supporting Information). In contrast, as exemplified with compound **4a**, alkyne derivatives displayed low hypochromism (as low as 8% for compound **4a**) upon binding to ct-DNA (Figure 3B).

On the basis of these UV−vis titration curves, the binding constants of all our newly synthesized compounds were determined using the neighbor exclusion model of McGhee and von Hippel as described in the Experimental Section. In all cases, the Scatchard plots (r/C_f vs r) revealed an obvious downward curvature of the plot which arises from the binding of a single molecule. This excluded the binding of other ligands nearby along the DNA polymer, a phenomenon also referred to as neighbor exclusion.[18] As can be seen from Table 1, the highest affinity toward ct-DNA was obtained with compound **3a**. The Scatchard plot analysis (Figure 3A, inset), also allowed us to determine the association constant K_a [$(3.24 \pm 0.3) \times 10^6$ M^{-1}] and the n parameter (6.8 ± 0.2), while standard Gibbs energy for the binding of compound **3a** with ct-DNA was found equal to −36.4 kJ mol^{-1}.

These results highlight the importance of the flexibility brought by the diaminopropyl linker and most probably a favorable interaction of the secondary and tertiary amine moieties with DNA. This hypothesis is corroborated by the high binding affinity of the other "Hoechst-amine" type ligands, such as compound **3b**, and, to a lesser extent, all the compounds bearing a diaminoethyl linker such as compounds **3c**, **3d**, and **3e**. Meanwhile, it is also interesting to point out the influence of the naphthalene moiety in **3b**, which appears to enhance the binding affinity in the amine series.

In contrast, all the ligands bearing an alkyne moiety were characterized by low affinities toward ct-DNA, thus showcasing that van der Waals interactions are not sufficient to counterbalance flexibility and electrostatic interactions. While having a low affinity toward ct-DNA, it could be noted that **4b** appears to be the most effective binder among the "Hoechst-alkyne" derivatives.

Another important factor was the degree of methoxy-substitution on the aromatic ring, which also appeared to enhance the DNA-binding affinity. As shown in Table 1, compound **3e**, which contains three methoxy groups attached to the aromatic ring, exhibited a higher affinity compared to compounds **3c** and **3d**, which contain one and two, respectively. This can be the result of the electron-donating properties of the methoxy substituents and perhaps favorable steric factors promoting the binding. This trend was also observed with compound **4c** bearing a pentamethyl-substituted aromatic ring. In addition, these results show that *para*-methoxy-substituted derivatives have a slightly higher affinity than the corresponding *meta*-substituted compounds (**4e** vs **4f**).

The binding of **3a**, **3b**, and **4b** was also studied in the presence of one equivalent $Cu(NO_3)_2$ for consistency purposes

DOI: 10.1021/acscatal.6b00495
ACS Catal. 2016, 6, 3096−3105

and in order to evaluate the influence of the copper ions on the binding of the ligands to ct-DNA. As can be seen from Table 1, the presence of Cu^{2+} ions reduces the binding constant of the ligands by 12, 21, and 9% for **3a**, **3b**, and **4b**, respectively. The effect of copper ions on ligand−DNA binding was reported earlier, and this decrease can be explained by the electrostatic interactions and coordination of the ligands by Cu^{2+}.[19]

Binding Study with Poly[d(A-T)$_2$]. The use of UV−vis absorbance spectroscopy allows us to unveil the binding properties of a given ligand toward specific base pairs in a DNA sequence.[13b,16f,20] In this context, we performed a series of UV−vis absorbance spectroscopy analyses of all our Hoechst-derivatives in the presence of the double strand alternating copolymer poly(deoxyadenylic-thymidylic) acid sodium salt, poly[d(A-T)$_2$], in order to ascertain a possible sequence specificity. As a general trend, the binding of these derivatives to poly[d(A-T)$_2$] was characterized by a hypochromic effect and a red shift similar to the ones observed with ct-DNA, albeit to a lesser extent (up to 35%). The high affinity of compound **3a** with poly[d(A-T)$_2$] was also confirmed (Figure 4); however,

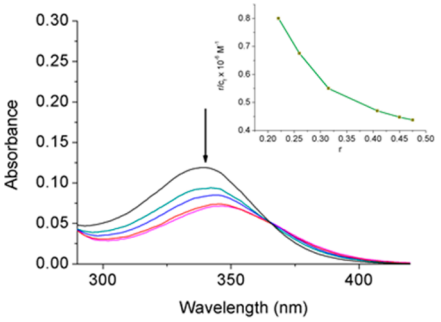

Figure 4. UV−vis absorption spectra of compound **3a** without (black curve) and in the presence of increasing concentration of poly[d(A-T)$_2$]. Inset: Scatchard plots for the binding of compounds **3a** with poly[d(A-T)$_2$] obtained from UV−vis titration data.

its binding constant with poly[d(A-T)$_2$] $(8.5 \pm 0.2) \times 10^5$ M^{-1} was lower than the one observed with ct-DNA. In addition, compound **3a** was shown to have an affinity 13.5 times lower than the unmodified Hoechst toward poly[d(A-T)$_2$] (Table 2). Interestingly, alkyne-type derivatives expressed a very low affinity toward poly[d(A-T)$_2$] showcased by a slight hypochromism effect in absorbance with even some hyperchromism effect detected for several compounds such as **4a**, **4e**, and **4f**. As a consequence, we limited the K_a determination to the amine-type derivatives.

Table 2. Spectroscopic Data and Association Constants Obtained for the Probe/Poly[d(A-T)$_2$] Mixture Study from UV−vis Titration (Cacodylate Buffer, pH 7.4, 25 °C)

compound	% hypochromism (wavelength/nm)	$K_a/10^5$, M^{-1}
3a	35 (341)	8.5(±0.3)
3b	23 (344)	5.2(±0.2)
3c	25 (340)	5.5(±0.1)
3d	26 (338)	7.2(±0.1)
3e	30 (343)	7.8(±0.1)
4a	−4 (355)[a]	n.d.
4b	7 (352)	n.d.
4c	1 (350)	n.d.
4d	2 (355)	n.d.
4e	−7 (347)[a]	n.d.
4f	−5 (349)[a]	n.d.
Hoechst 33258	45 (340)	114.8 (±5)

[a]Negative values refer to hyperchromism.

The high binding constants toward poly[d(A-T)$_2$] displayed by compounds **3a** and **3e** confirmed their high affinity toward AT base pairs and the steric and electronic effects that promote the binding. Similarly, comparing compounds **3c**, **3d**, and **3e**, all bearing one or multiple methoxy groups on the benzylic ring, indicate that the methoxy substituents do not affect the AT-base recognition of the ligands.

Another important outcome of this study was the fact that these compounds were characterized by a low binding constant with poly[d(A-T)$_2$] compared to ct-DNA, which we believe is related to their high GC recognition ability. Hence, the absence of GC base pairs causes a significant decrease in binding constants (and binding site size). This GC-specificity will be later confirmed by molecular docking studies.

Fluorescence Measurements. Fluorescence emission measurements were performed to describe the sequence-specificity of compound **3a**, which was found to be the best binder to ct-DNA and poly[d(A-T)$_2$] following the UV−vis experiments. For this purpose, a 1 μM solution of ligand **3a** was titrated individually with five different 28-mer DNA hairpins with sequences having the following structure: 5′-d-(CGCG**X**CGCGTTTTCGCG**X**CGCG)-3′, where **X** represents the part of the hairpin which varies (X = ATAT, TAAT, TATA, TTAA, and AATT). On the basis of the fluorescence measurements, we were able to determine the strongest and the weakest binding sites for **3a**. Figure 5 presents the fluorescence spectra of compound **3a** titrated with DNA hairpins with **X** = AATT (strongest binding site) and **X** = TATA (weakest binding site). Fluorescence titration spectra for the three other sequences are given in the Supporting Information. Fluorescence titration results for all five sequences were analyzed by plotting the relative fluorescence increase $(F - F_0)/F_0$ vs [ligand:DNA] ratio. The highest increase in fluorescence was observed for AATT, whereas the lowest was observed for TATA (Figure 6). In all cases, however, the saturation limit was reached at a 1:1 ligand/DNA ratio, which means that the ligand binds to the DNA in a monomeric form. In addition, all the fluorescence experiments revealed that the affinity of **3a** increased depending on the base sequences (TATA < TTAA < TAAT < ATAT < AATT), which was in agreement with the sequence specificity exhibited by Hoechst 33258.[16e,17b]

Thermal Melting Study. Thermal melting studies were undertaken to describe the relative binding affinity and the sequence selectivity of the ligands toward DNA.[21] Indeed, DNA denaturation is usually associated with a hyperchromic effect in the absorbance, which is temperature-dependent. All compounds that bind to DNA give rise to a stabilization of the DNA visualized by an increase of the melting temperature denoted T_m. Conversely, a decrease in T_m is indicative of a distortion induced by the DNA binder. On the basis of fluorescence results which revealed that these derivatives have a higher affinity toward the AATT sequence, we performed a melting analysis with the 20-mer hairpin 5′-d-(CGAATTCGTTTTCGAATTCG)-3′. Melting measurements were performed by monitoring the absorbance of the hairpins solutions at 260 nm in the absence (the T_m value of the free sequence is 67.1 °C) and the presence of one equiv of compounds **3a−d** (benzyl amine-type derivatives), compounds

DOI: 10.1021/acscatal.6b00495
ACS Catal. 2016, 6, 3096−3105

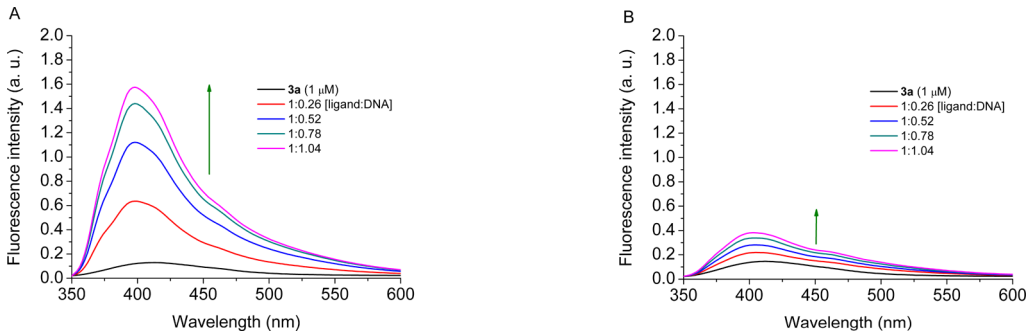

Figure 5. Fluorescence emission spectra for **3a** titrated with AATT (A) and with TATA (B): 1 μM solution of **3a** in 10 mM sodium cacodylate-100 mM NaCl, pH 7.4 buffer at 25 °C, excitation wavelength was set at 341 nm, which is λmax for the free ligand. The changes in ligand:DNA ratio for both cases fall in the same region (1:0−1:1.04). Under these concentration conditions, **3a** is fully bound to the DNA at the highest concentration shown in the figures.

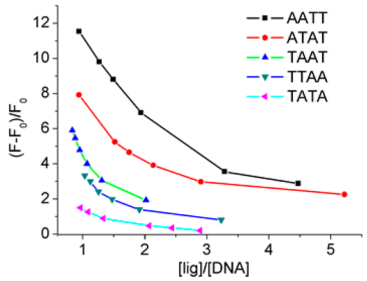

Sequence	$K_a/10^6$, M^{-1}
AATT	11.15
ATAT	7.62
TAAT	5.78
TTAA	3.05
TATA	1.85

Figure 6. Relative fluorescence intensity increase of the compound **3a** as a function of [ligand]/[DNA] ratio for five different DNA sequences.

4b and **4e** (propargyl alkyne type derivatives), and Hoechst 33258 as a reference. Melting temperatures were determined from the first derivatives of the melting curves and summarized in Table 3. As a general trend, compounds **3a** and **3b** showed

Table 3. Thermal Melting Studies of the Designed Hoechst Derivatives with 20-mer DNA Hairpin 5′-d(CGAATTCGTTTTCGAATTCG)-3′[a]

compound	T_m (°C)	ΔT_m (°C)
3a	74.3	7.2
3b	74.1	7.0
3c	70.2	3.1
3d	70.6	3.5
3e	70.8	3.7
4b	68.9	1.8
4e	68.3	1.2
Hoechst 33258	74.5	7.4

[a] $\Delta T_m = T_m$ (complex) − T_m (free DNA). The listed values are for a 1:1 [ligand]/[DNA] ratio and an average of two independent experiments with a reproducibility of ±0.5 °C.

the highest DNA-stabilizing effect among all the Hoechst derivatives (ΔT_m = 7.2 and 7.0 °C, respectively) almost identical to the stabilization induced by Hoechst 33258 and in good agreements with their binding constant values obtained by UV−vis titration experiments. Compounds with an ethylamine type linker (**3e**, **3d**, and **3c**) showed a moderate increase in DNA stability (ΔT_m = 3.7, 3.5, and 3.1 °C, respectively). Conversely, compound **4e** did not show any significant enhancement. These results confirm the importance of the aminopropyl linker compared to the aminoethyl one as well as a necessary flexibility for efficient groove binding. Introducing the aminopropyl-type linker clearly increased the conformational mobility of **3a** and **3b** and opened up the space for the binding of the pyridine and the methoxybenzyl moieties linked to the Hoechst residue. This linkage most probably promotes the H-bonding between the ligands and the DNA bases. Meanwhile, the results substantiate the role played by the methoxy substituents on the benzyl ring.

Circular Dichroism Measurements. In order to characterize the type of interaction between our ligands and DNA, we performed a set of circular dichroism spectroscopy experiments.[22] Indeed, compared to intercalative interactions, minor groove binders induce larger CD signals. Moreover, neither ct-DNA nor the free compounds exhibit CD signals above 300 nm. Monitoring induced CD, binding mode, and saturation limit for selected compound **3a** were performed by CD titration experiments as a function of compound concentration. Addition of **3a** to ct-DNA resulted in significant positive induced CD signals on complex formation with DNA at the wavelength between 300 and 400 nm. The CD spectra of ct-DNA and its complexes with **3a** at dye/DNA base pairs mixing ratios varying from 0 to 0.15 are shown in Figure 7. Notably, ICD peaks positions of **3a** matched the absorption peak positions of bound probes (Table 1), thus indicating that these ICD peaks correspond to the same chromophore, which is responsible for the red-shifted absorption spectra shown Figure 3.

Changes of ICD intensities of **3a** at 350 nm are illustrated in Figure 7, inset. The CD signals of ct-DNA around 245 and 280 nm are decreasing in intensity with a saturation limit for compound **3a** reached at ligand/DNA ratio of 0.15 in good agreement with UV−vis absorption titration data. This is indicative of a binding density value n = 6.8 corresponding to a dye/DNA ratio equal to 1/6.8 = 0.147. Hence, CD spectroscopy measurements revealed the minor groove binding

DOI: 10.1021/acscatal.6b00495
ACS Catal. 2016, 6, 3096−3105

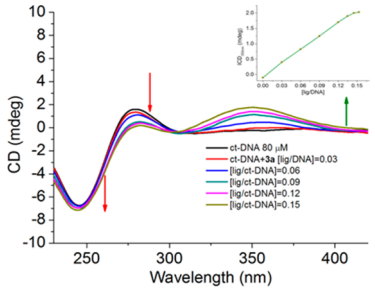

Figure 7. Circular dichroism spectra of representative compound **3a** with ct-DNA. Mixing ratios of ligand to ct-DNA base pairs are 0, 0.03, 0.06, 0.09, 0.12, and 0.15. Color arrows indicate positive (green) and negative (red) induced changes. The experiments were conducted in cacodylate buffer at 25 °C. Inset picture is the change of ICD intensities of **3a** at 350 nm during titration with ct-DNA. Ligand/DNA base pairs ratio was varied from 0 to 0.15.

character of the representative compound **3a** and confirmed the saturation limit obtained from UV−vis measurements.

Molecular Modeling Studies. To better understand the binding of **3a** to DNA and to reveal the most probable conformations in which the ligand binds to DNA, we performed molecular docking studies. The initial DNA duplex selected for docking was dodecamer 5′-d-(CGCGAATTCGCG)-3′ (PDB ID: 1BNA). Docking results are presented in Figure 8. A detailed view of the diamine part of compound **3a** in docked conformation is shown in Figure 9.

For compound **3a**, the docking program identified nine possible conformations with values of affinity comprised between −54.8 and −47.88 kJ mol^{-1}. Docking results revealed the possibility of hydrogen-bonding interactions between the inner facing benzimidazole N−H group and AT bases of DNA in the floor of the minor groove of DNA, which is typical for benzimidazole-containing drugs of the Hoechst 33258 family.[23] Additionally, docking results showed the possibility of H-bond forming between the nitrogen atom of the methylpyridine and the G-NH_2 moiety, which support the G-recognition ability of compound **3a** obtained from UV−vis absorption measurements. The H-bond acceptor property of the pyridine nitrogen atom is a well-established phenomenon.[24] Hydrogen bonds are shown in Figure 10, and the length of the hydrogen bonds determined with PyMOL software are given in Table 4.

DNA-Based Asymmetric Catalysis. To demonstrate the efficacy of our bifunctional Hoechst-derived ligands, amine-type **3a** and **3b** and alkyne-type **4b** derivatives were selected and engaged in the copper-catalyzed Friedel−Crafts alkylation of α,β-unsaturated 2-acyl imidazole **11** with 5-methoxyindole **12**. The experiments were conducted at 5 °C using a stock solution of a Cu(II)-ligand complex (in MOPS 20 mM, pH 6.5) and DNA (2 mM in MOPS 20 mM, pH 6.5). The results are reported in Table 5. 4,4′-Dimethyl-2,2′-bipyridine (**bmbpy**) was also used as a control.

As a general trend, the ligand concentration had a non-negligible impact on the enantioselectivity of the reaction; the best ee values were obtained at a 0.1 mM concentration (Table 5, entries 1 and 2). Interestingly, this phenomenon was not observed when using an intercalating ligand such as 4,4′-dimethyl-2,2′-bipyridine. In the presence of ct-DNA, we were pleased to observe a significant induction, in particular with **3b**, albeit not in the range of the one obtained when using dmbpy. In contrast, with low binding alkyne-type ligands such as **4b**, the ee value decreased sharply to 7%, thus confirming that the affinity of the ligand had a significant impact on the enantioselectivity outcome of the reaction (Table 5, entries 1−4). Interestingly, in the presence of the AATT hairpin, the enantioselectivity decreased from +80% to +31% with **dmbpy**. Although the exact reason for this sharp decrease is still unclear, we were pleased to observe an unexpected inversion of selectivity with the groove binder ligands **3a** (from +29% to −16%) and **3b** (from +47% to −26%) (Table 5, entries 5−8) which was also observed with the TATA hairpin (Table 5, entries 9−12).

These results clearly validate the groove-binder anchoring strategy in the context of DNA-based asymmetric catalysis. Even though it is evident that a simple affinity/enantioselectivity correlation cannot be categorical, we have confirmed that derivatives such as **3** were the strongest binding ligands and that AATT was the best binding site. A precise tuning of the binder/DNA complex (optimal binding position and orientation of the ligand, flexibility of the linker, $(A/T)_n$ sites that modulate the minor groove width and most probably flanking

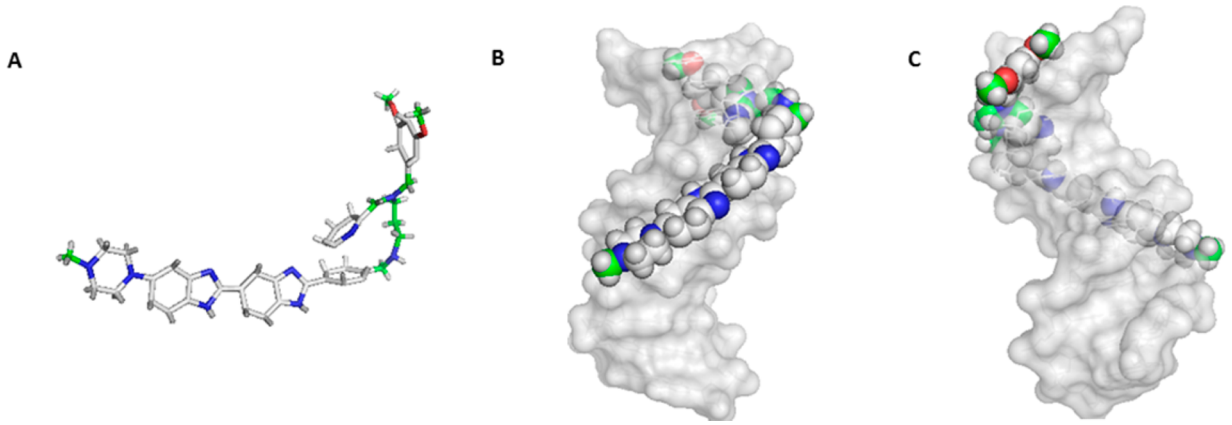

Figure 8. Molecular models for **3a** docked into the $d(CGCGAATTCGCG)_2$ sequence. (A) Conformation of compound **3a** (obtained from docking results) in which it has a higher affinity toward the DNA dodecamer. View from the minor (B) and the major groove (C) of compound **3a** docked in the minor groove of DNA. These images are the ones of the lowest-energy conformation and have been drawn with the PyMOL software. The transparency of the molecular surface of DNA dodecamer is shown with 60% transparency. Note that the surface of **3a** and the surface of minor groove wall of DNA are in close contact.

DOI: 10.1021/acscatal.6b00495
ACS Catal. 2016, 6, 3096−3105

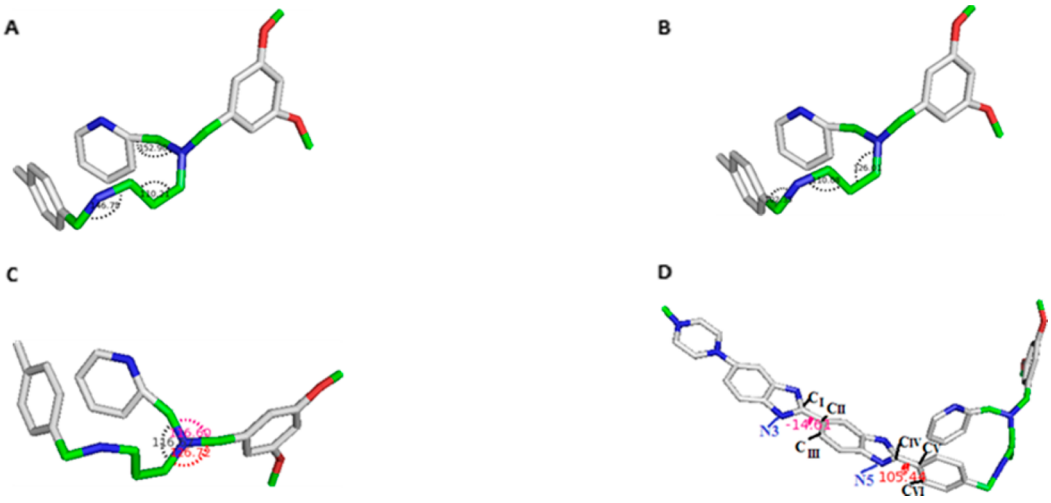

Figure 9. Structural properties of compound **3a** in docked conformation: (A,B,C) Angles between bonds of diamine moiety of compound **3a**. (D) Dihedral angles N3CICIICIII and N5CIVCVCVI. The angles are shown as dashed arc lines. Three different pictures (A–C) of the same moiety were drawn for clarity. Angles between bonds were determined from docked conformation of **3a** using the PyMOL software.

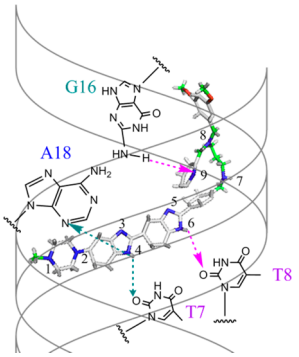

Figure 10. Detailed view from the minor groove of the hydrogen-bond interactions between compound **3a** (shown as dashed arrows) and DNA bases. Data are based on zoomed-in (30×) view of docking results as presented in Figure 8. For clarity purposes, only the bases which participate through H-bonding interaction with the ligand are shown. Shown hydrogen bonds are the following: between nitrogen atoms of inner-facing benzimidazole N–H groups: I. N4 hydrogen atom of **3a** and N3 atom of adenine 18, II. N4 hydrogen atom of **3a** with O2 atom of T7 (I and II are equally probable H bonds), III. N6 hydrogen atom of **3a** and O2 atom of T8, IV. H-bond between N9 of **3a** and NH2 group of G16.

Table 4. Ligand–DNA Hydrogen-Bond Distances in the 3a–d(CGCGAATTCGCG)$_2$ Complex

3a atom	DNA atom	distance (Å)
H of N4	O2 (T7)	3.1
H of N4	N3 (A18)	2.9
H of N6	O2 (T8)	3.2
N9	H of NH2 (G16)	3.0

bases) is now essential to attain higher levels of enantioselectivity.

CONCLUSION

The design and synthesis of compounds exhibiting a high affinity toward DNA sequences has been successfully achieved on the basis of structural modifications brought to the well-known minor groove binder Hoechst 33258. Analysis based on UV–vis titration and thermal denaturation, as well as

Table 5. Friedel–Crafts Alkylation Using Hoechst-Derived Ligands 3a, 3b, and 4b

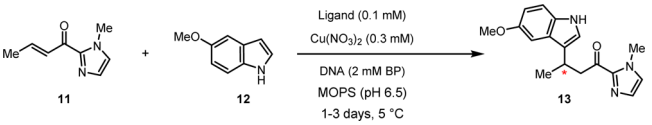

entry	ligand	DNA	conversion (%)[a]	ee (%)[a]
1	**dmbpy**	ct-DNA	>99	(+) 80
2	**3a**	ct-DNA	>99	(+) 29
3	**3b**	ct-DNA	>99	(+) 47
4	**4b**	ct-DNA	94	(+) 7
5	**dmbpy**	ODN-**1**	>99	(+) 31
6	**3a**	ODN-**1**	>99	(−) 16
7	**3b**	ODN-**1**	78	(−) 26
8	**4b**	ODN-**1**	>99	(+) 4
9	**dmbpy**	ODN-**2**	>99	(+) 43
10	**3a**	ODN-**2**	72	(−) 19
11	**3b**	ODN-**2**	>99	(−) 23
12	**4b**	ODN-**2**	>99	(−) 5

[a]Determined by supercritical fluid chromatography (SFC) analysis. [ODN-**1** = 5′-d(CGAATTCGTTTTCGAATTCG)-3′, [ODN-**2**] = 5′-d(CGTATACG TTTTCGTATACG)-3′].

fluorescence and CD experiments showed that compounds with an alkyne type linkage showed low affinity toward ct-DNA and poly[d(A-T)$_2$] compared to their corresponding amine analogues. This was most probably preconditioned by the low flexibility of the triple bond, which impedes favorable interactions between the pyridine and the methoxybenzyl groups with the DNA bases. Also, it is probably the absence of one charged nitrogen atom in the alkyne-type derivatives (compared with the amine-type derivatives), which reduces the strength of the electrostatic interactions between the ligand and the DNA phosphate backbone and thus weakens the affinity of the ligand toward DNA. Meanwhile, designed derivatives bearing a diaminoalkyl linker and especially the diaminopropyl tether appeared to have a high affinity toward both ct-DNA and poly[d(A-T)$_2$], which confirms the potential of our minor-groove-binder anchoring strategy. The results presented in this work clearly show that a rational design of Hoechst derivatives

DOI: 10.1021/acscatal.6b00495
ACS Catal. 2016, 6, 3096–3105

capable of binding to mixed DNA sequences is possible and that a groove binder anchoring strategy for DNA-based asymmetric catalysis is valuable to achieve sequence-selective reactions. The inversion of enantioselectivity observed with AT-rich sequences extends the tools available until now to control the enantioselectivity outcome of a DNA-catalyzed reaction.[25] The success of Hoechst 33258-amine type derivatives having mixed DNA sequence recognition capabilities such as **3a** and **3b** offers exciting prospects for DNA-based asymmetric catalysis.

EXPERIMENTAL SECTION

Ligands and DNA Oligonucleotides. Hoechst 33258, ct-DNA, and poly[d(A-T)$_2$] were purchased from Sigma-Aldrich (U.S.A.). For the preparation of the Hoechst derivatives solutions, all the compounds were carefully weighed and dissolved in a methanol solution containing 5% (v/v) of 0.1 mM HCl. Concentrations of Hoechst 33258, ct-DNA, poly[d(A-T)$_2$], and DNA hairpins were determined spectroscopically using the following extinction coefficients: ε_{338} = 42 000 M^{-1} cm^{-1} for Hoechst 33258, ε_{260} = 13 200 M^{-1} cm^{-1} for ct-DNA concentration expressed as base pairs, ε_{262} = 13 600 M^{-1} cm^{-1} for poly[d(A-T)$_2$] concentration as base pairs. For DNA hairpins, the extinction coefficients provided by the supplier were used. All the solutions used for spectroscopic titrations were prepared in sodium cacodylate buffer containing 10 mM sodium cacodylate and 100 mM NaCl at pH 7.4. Milli-Q water was used for the preparation of all the solutions. The binding studies were carried out at 25 °C.

UV-Spectrophotometry. UV−vis scanning and melting measurements were performed using Varian Cary 300 Bio spectrophotometer equipped with Peltier temperature control system using 1 cm path length quartz cells. A solution of probe (4 μM, 1 mL, cacodylate buffer) was titrated by adding 5 μL increments of nucleic acid (1 mM) while monitoring the absorbance in the 200−420 nm region. The total volume of nucleic acid during the titration did not exceed 10% of the initial volume, and spectra were corrected for small changes in volume during the titration. The absorption data for all derivatives were analyzed according to neighbor exclusion model of McGhee and von Hippel[26] using eq 1. The binding-constant values were estimated from nonlinear regression analysis. All data were treated using OriginPro8 software.

$$r/C_f = K_a[1 - nr(1 - nr)]/[1 - (n - 1)r]^{n-1} \quad (1)$$

In eq 1, C_f is the concentration of the free probe, n is the binding density, and r is the ratio of concentration of bound probe (C_b) to that of DNA. Based on absorbance titration, the values of C_f were calculated using eq 2, where A_{obs} is the absorbance at the peak position of the ligand-DNA mixture, C_t is the total concentration of the probe, ε_f and ε_b are the extinction coefficients of the free and bound probes, respectively. The value of ε_b was estimated from a half reciprocal plot of A_{obs} versus 1/[DNA]. The percent hypochromism was calculated as equal to $(1 - \varepsilon_b/\varepsilon_f)\cdot 100\%$.

$$C_f = (A_{obs} - \varepsilon_b C_t)/(\varepsilon_f - \varepsilon_b) \quad (2)$$

The free energy of binding ($\Delta G°$) was calculated using eq 3.

$$\Delta G° = -RT \ln K_a \quad (3)$$

Circular Dichroism Spectroscopy (CD). Circular dichroism spectroscopy experiments were performed on a Jasco 815 model spectrophotometer in 1 cm quartz cell at 25 °C. Prior to all measurements, a buffer spectra was recorded for blank correction. A solution of calf thymus DNA (80 μM) in buffer (10 mM sodium cacodylate, 100 mM NaCl, pH 7.4) was added to the cell prior to the experiment followed by the solution of **3a** (0.48 mM in MeOH containing 5% (v/v) of 0.1 mM HCl) in 5 μL increments. The resulting solution was incubated for 10 min to achieve the equilibrium binding for the DNA complex. Each spectrum presents the average of three scans from 220 to 420 nm with a scan speed 60 nm·min^{-1} and a response time of 1 s.

Fluorescence Emission Spectroscopy. Fluorescence spectra were recorded on a Jasco 815 model spectrophotometer using 1 cm path length quartz cells. Excitation and emission bandwidths were fixed at 2 and 10 nm, respectively. A solution of ligand **3a** at a concentration of 1 μM was prepared in a 10 mM sodium cacodylate/100 mM NaCl buffer (pH 7.4) and hairpin DNA aliquots (5 μL increments) were added from a concentrated stock (52 μM in a cacodylate buffer). The spectra were collected after allowing an equilibration time of 10 min. Compound **3a** was excited at 341 nm, which is λ_{max} for the free ligand as identified by UV−vis spectroscopy. Emission spectra were monitored from 350 to 600 nm. All the fluorescence titrations were performed at 25 °C.

Molecular Docking Studies. The crystal structure of the synthetic DNA dodecamer 5′-d(CGCGAATTCGCG)-3′ has been refined to a residual error of R = 17.8% at 1.9 Å resolution (two-sigma data). The molecule forms slightly more than one complete turn of a right-handed double-stranded B helix.[27] AutoDock Vina was used for docking experiments.[28] PDB files for the ligand structures were created using Open Babel graphical user interface 2.3.1.[29] PDBQT molecular structure files necessary for AutoDock Vina were created using AutoDock Tools graphical user interface.[30] Water molecules were deleted, and hydrogen atoms were added before creating PDBQT files. Kollman all-atom charges for DNA and Gasteiger−Hükel charges for the ligand were computed. PyMOL software was used to visualize the docking results. All modeling studies were carried out on a windows workstation. The following parameters were used during docking with AutoDock Vina: search space center x = 10.9, center y = 22.0, center z = 8.9 (these coordinates allow for the grid box center to be in the minor groove), search space sizes: size x = 70, size y = 65, size z = 80, spacing 1 Å. Both the ligand and the bound DNA were permitted torsional flexibility in the docking process.

DNA-Based Asymmetric Catalysis Experiments. To a 2 mM DNA solution in a 20 mM MOPS buffer (600 μL, pH 6.5) was added the stock solution of [Cu(Hoechst-derived ligand)(NO$_3$)$_2$]. The resulting DNA solution was cooled to 5 °C. To the mixture was then added a 0.5 M solution of enone in MeCN (1.2 μL), followed by the 5-methoxyindole (**12**). The reaction was mixed by inversion at 5 °C in a cold room. After 1−3 days, the mixture was warmed to room temperature and extracted with Et$_2$O (3 × 2 mL). The combined organic layers were washed with brine (2 × 5 mL), dried over Mg$_2$SO$_4$, gravity filtered, and concentrated under reduced pressure to give the crude product, which was subjected to supercritical fluid chromatography (SFC) analysis.

DOI: 10.1021/acscatal.6b00495
ACS Catal. 2016, 6, 3096−3105

■ ASSOCIATED CONTENT

Supporting Information

The Supporting Information is available free of charge on the ACS Publications website at DOI: 10.1021/acscatal.6b00495.

Experimental procedures as well as spectroscopic and analytical data (PDF)

■ AUTHOR INFORMATION

Corresponding Authors

*E-mail for S.A.: s.arseniyadis@qmul.ac.uk.
*E-mail for M.S.: msmietana@um2.fr.

Notes

The authors declare no competing financial interest.

■ ACKNOWLEDGMENTS

We thank the Ministère de l'Enseignement Supérieur et de la Recherche, the Agence Nationale de la Recherche (D-CYSIV Project; ANR-2015-CE29-0021-01) and the Erasmus Mundus Backis Program for their support.

■ REFERENCES

(1) (a) Dürrenberger, M.; Ward, T. R. *Curr. Opin. Chem. Biol.* **2014**, *19*, 99−106. (b) Hoarau, M.; Hureau, C.; Gras, E.; Faller, P. *Coord. Chem. Rev.* **2016**, *308*, 445−459.

(2) Bos, J.; Roelfes, G. *Curr. Opin. Chem. Biol.* **2014**, *19*, 135−143.

(3) Roelfes, G.; Feringa, B. L. *Angew. Chem., Int. Ed.* **2005**, *44*, 3230−3232.

(4) (a) Coquiere, D.; Feringa, B. L.; Roelfes, G. *Angew. Chem., Int. Ed.* **2007**, *46*, 9308−9311. (b) Dijk, E. W.; Boersma, A. J.; Feringa, B. L.; Roelfes, G. *Org. Biomol. Chem.* **2010**, *8*, 3868−3873. (c) Dijk, E. W.; Feringa, B. L.; Roelfes, G. *Tetrahedron: Asymmetry* **2008**, *19*, 2374−2377. (d) Boersma, A. J.; Coquiere, D.; Geerdink, D.; Rosati, F.; Feringa, B. L.; Roelfes, G. *Nat. Chem.* **2010**, *2*, 991−995. (e) Boersma, A. J.; Feringa, B. L.; Roelfes, G. *Angew. Chem., Int. Ed.* **2009**, *48*, 3346−3348. (f) Boersma, A. J.; Klijn, J. E.; Feringa, B. L.; Roelfes, G. *J. Am. Chem. Soc.* **2008**, *130*, 11783−11790. (g) Oelerich, J.; Roelfes, G. *Chem. Sci.* **2013**, *4*, 2013−2017. (h) Shibata, N.; Yasui, H.; Nakamura, S.; Toru, T. *Synlett* **2007**, *2007*, 1153−1157. (i) Boersma, A. J.; Megens, R. P.; Feringa, B. L.; Roelfes, G. *Chem. Soc. Rev.* **2010**, *39*, 2083−2092. (j) Garcia-Fernandez, A.; Roelfes, G. *Met. Ions Life Sci.* **2012**, *10*, 249−268. (k) Park, S.; Ikehata, K.; Watabe, R.; Hidaka, Y.; Rajendran, A.; Sugiyama, H. *Chem. Commun.* **2012**, *48*, 10398−10400. (l) Li, Y.; Wang, C.; Jia, G.; Lu, S.; Li, C. *Tetrahedron* **2013**, *69*, 6585−6590.

(5) Wang, J.; Benedetti, E.; Bethge, L.; Vonhoff, S.; Klussmann, S.; Vasseur, J.-J.; Cossy, J.; Smietana, M.; Arseniyadis, S. *Angew. Chem., Int. Ed.* **2013**, *52*, 11546−11549.

(6) Benedetti, E.; Duchemin, N.; Bethge, L.; Vonhoff, S.; Klussmann, S.; Vasseur, J.-J.; Cossy, J.; Smietana, M.; Arseniyadis, S. *Chem. Commun.* **2015**, *51*, 6076−6079.

(7) (a) Petrova, G. P.; Ke, Z.; Park, S.; Sugiyama, H.; Morokuma, K. *Chem. Phys. Lett.* **2014**, *600*, 87−95. (b) Rosati, F.; Boersma, A. J.; Klijn, J. E.; Meetsma, A.; Feringa, B. L.; Roelfes, G. *Chem. - Eur. J.* **2009**, *15*, 9596−9605.

(8) (a) Boersma, A. J.; de Bruin, B.; Feringa, B. L.; Roelfes, G. *Chem. Commun.* **2012**, *48*, 2394−2396. (b) Draksharapu, A.; Boersma, A. J.; Browne, W. R.; Roelfes, G. *Dalton Trans.* **2015**, *44*, 3656−3663. (c) Draksharapu, A.; Boersma, A. J.; Leising, M.; Meetsma, A.; Browne, W. R.; Roelfes, G. *Dalton Trans.* **2015**, *44*, 3647−3665.

(9) (a) Gjonaj, L.; Roelfes, G. *ChemCatChem* **2013**, *5*, 1718−1721. (b) Park, S.; Zheng, L.; Kumakiri, S.; Sakashita, S.; Otomo, H.; Ikehata, K.; Sugiyama, H. *ACS Catal.* **2014**, *4*, 4070−4073. (c) Fournier, P.; Fiammengo, R.; Jäschke, A. *Angew. Chem., Int. Ed.* **2009**, *48*, 4426−4429. (d) Oltra, N. S.; Roelfes, G. *Chem. Commun.* **2008**, *45*, 6039−6041.

(10) (a) Maher, L. J.; Dervan, P. B.; Wold, B. *Biochemistry* **1992**, *31*, 70−81. (b) Giovannangeli, C.; Perrouault, L.; Escude, C.; Thuong, N.; Helene, C. *Biochemistry* **1996**, *35*, 10539−10548. (c) Giovannangeli, C.; Helene, C. *Antisense Nucleic Acid Drug Dev.* **1997**, *7*, 413−421.

(11) Wang, G.; Seidman, M. M.; Glazer, P. M. *Science* **1996**, *271*, 802−805.

(12) Broitman, S.; Amosova, O.; Dolinnaya, N. G.; Fresco, J. R. *J. Biol. Chem.* **1999**, *274*, 21763−21768.

(13) (a) Zimmer, C.; Wahnert, U. *Prog. Biophys. Mol. Biol.* **1986**, *47*, 31−112. (b) Loontiens, F. G.; Regenfuss, P.; Zechel, A.; Dumortier, L.; Clegg, R. M. *Biochemistry* **1990**, *29*, 9029−9039. (c) Dervan, P. B. *Science* **1986**, *232*, 464−471.

(14) Henderson, D.; Hurley, L. H. *Nat. Med.* **1995**, *1*, 525−527.

(15) (a) Chen, A. Y.; Yu, C.; Gatto, B.; Liu, L. F. *Proc. Natl. Acad. Sci. U. S. A.* **1993**, *90*, 8131−8135. (b) Beerman, T. A.; McHugh, M. M.; Sigmund, R.; Lown, J. W.; Rao, K. E.; Bathini, Y. *Biochim. Biophys. Acta, Gene Struct. Expression* **1992**, *1131*, 53−61.

(16) (a) Teng, M.; Usman, N.; Frederick, C. A.; Wang, A. H. J. *Nucleic Acids Res.* **1988**, *16*, 2671−2690. (b) Squire, C. J.; Baker, L. J.; Clark, G. R.; Martin, R. F.; White, J. *Nucleic Acids Res.* **2000**, *28*, 1252−1258. (c) Pjura, P. E.; Grzeskowiak, K.; Dickerson, R. E. *J. Mol. Biol.* **1987**, *197*, 257−271. (d) Fede, A.; Billeter, M.; Leupin, W.; Wuthrich, K. *Structure* **1993**, *1*, 177−186. (e) Breusegem, S. Y.; Clegg, R. M.; Loontiens, F. G. *J. Mol. Biol.* **2002**, *315*, 1049−1061. (f) Breusegem, S. Y.; Sadat-Ebrahimi, S. E.; Douglas, K. T.; Clegg, R. M.; Loontiens, F. G. *J. Mol. Biol.* **2001**, *308*, 649−663.

(17) (a) Harshman, K. D.; Dervan, P. B. *Nucleic Acids Res.* **1985**, *13*, 4825−4835. (b) Abu-daya, A.; Brown, P. M.; Fox, K. R. *Nucleic Acids Res.* **1995**, *23*, 3385−3392.

(18) Dedon, P. C. *Curr. Protoc. Nucleic Acid Chem.* **2000**, Unit 8.2.1−8.2.8.

(19) Barone, G.; Terenzi, A.; Lauria, A.; Almerico, A. M.; Leal, J. M.; Busto, N.; Garcia, B. *Coord. Chem. Rev.* **2013**, *257*, 2848−2862.

(20) Bailly, C.; Colson, P.; Hénichart, J. P.; Houssier, C. *Nucleic Acids Res.* **1993**, *21*, 3705−3709.

(21) (a) Wilson, W. D.; Tanious, F. A.; Fernandez-Saiz, M.; Rigl, C. T. *Methods Mol. Biol.* **1997**, *90*, 219−240. (b) Akashi, S. *Med. Res. Rev.* **2006**, *26*, 339−368. (c) Rettig, M.; Kamal, A.; Ramu, R.; Mikolajczak, J.; Weisz, K. *Bioorg. Med. Chem.* **2009**, *17*, 919−928.

(22) (a) Norden, B.; Kubista, M.; Kurucsev, T. Q. *Q. Rev. Biophys.* **1992**, *25*, 51−170. (b) Karlsson, H. J.; Eriksson, M.; Perzon, E.; Akerman, B.; Lincoln, P.; Westman, G. *Nucleic Acids Res.* **2003**, *31*, 6227−6234.

(23) Clark, G.; Boykin, D.; Czarny, A.; Neidle, S. *Nucleic Acids Res.* **1997**, *25*, 1510−1515.

(24) (a) Li, T.; Zhou, P.; Mattei, A. *CrystEngComm* **2011**, *13*, 6356−6360. (b) Du, Y.; Du, X.; George, S. *J. Phys. Chem. C* **2007**, *111*, 219−226.

(25) Rioz-Martínez, A.; Roelfes, G. *Curr. Opin. Chem. Biol.* **2015**, *25*, 80−87.

(26) McGhee, J. D.; von Hippel, P. H. V. *J. Mol. Biol.* **1974**, *86*, 469−489.

(27) Drew, H. R.; Wing, R. M.; Takano, T.; Broka, C.; Tanaka, S.; Itakura, K.; Dickerson, R. E. *Proc. Natl. Acad. Sci. U. S. A.* **1981**, *78*, 2179−2183.

(28) Trott, O.; Olson, A. J. *J. Comput. Chem.* **2010**, *31*, 455−461.

(29) O'Boyle, N. M.; Banck, M.; James, C. A.; Morley, C.; Vandermeersch, T.; Hutchison, G. R. *J. Cheminf.* **2011**, *3*, 33.

(30) Morris, G. M.; Huey, R.; Lindstrom, W.; Sanner, M. F.; Belew, R. K.; Goodsell, D. S.; Olson, A. J. *J. Comput. Chem.* **2009**, *30*, 2785−2791.

DOI: 10.1021/acscatal.6b00495
ACS Catal. 2016, 6, 3096−3105